Energy dissipation of a sphere rolling up a granular slope: Slip and deformation of the granular surface

T. Fukumoto, K. Yamamoto, M. Katsura, and H. Katsuragi

Department of Earth and Space Science, Osaka University, 1-1 Machikaneyama, Toyonaka 560-0043, Japan

We experimentally investigate the dynamics of a sphere rolling up a granular slope. During the rolling-up motion, the sphere experiences slipping and penetration (groove formation) on the surface of the granular layer. The former relates to the stuck motion of the rolling sphere, and the latter causes energy dissipation due to the deformation of the granular surface. To characterize these phenomena, we measured the motion of a sphere rolling up a granular slope of angle α. The initial velocity v_0, initial angular velocity ω_0, angle of slope α, and density of the sphere ρ_s were varied. As a result, the penetration depth can be scaled solely by the density ratio between the sphere and granular layer. By considering the rotational equation of motion, we estimate the friction due to the slips. Besides, by considering energy conservation, we define and estimate the friction due to groove formation. Moreover, the translational friction is proportional to the penetration depth. Using these results, we can quantitatively predict the sphere's motion including stuck behavior.

I. INTRODUCTION

In general, granular bed is so deformable that various phenomena such as impact cratering [1] and wedge formation by plowing [2] can be induced. Granular deformability enables us to draw even sand art [3]. We focus on a certain type of deformation and related frictional phenomenon occurring on the granular surface. Specifically, on loose sand surfaces, vehicles might be stuck by the wheels spinning out. Preventing such stuck behavior is a key of efficient vehicle design. The wheel-stuck phenomena can induce severe malfunction of the planetary explorer as well. For example, the Mars rover, Spirit, was stuck on the surface of Mars. After that, Spirit could not continue the exploration of the Martian environment [4]. Efficient vehicle design is the main topic in the field of terramechanics research. Particularly, the slip ratio of the rover's wheel that depends on the shape and driving conditions of the rover has been studied extensively [5,6]. The principal goal of these terramechanics researches is developing high-performance rovers. Thus, the specific geometry and setup of the rover have been studied.

However, a fundamental understanding of the relationship between a granular surface and a simple object (such as a sphere) has not been sufficient. Investigation of such a fundamental relation could also relate to the ecology of antlions that use the stuck phenomena to prey on ants [7,8]. It would also relate to groove formation on planetary granular surfaces. For example, traces of boulder falls on the regolith layer have been found [9,10]. To discuss the mechanics of such boulder-fall traces, the interaction between a granular surface and a macroscopic object must be revealed. Namely, while the setup we consider—rolling sphere on a granular slope—is quite simple, it relates to various phenomena such as vehicle design (engineering), ecology of antlions, and planetary surface processes.

For a proper understanding of the interaction between a solid object and a granular surface, frictional property is the most important factor. Since granular frictional behaviors are quite diverse and complex, various efforts have been made to reveal the constitutive law of granular friction (e.g., Refs. [11–13]). Regarding the interaction between granular matter and objects, various friction-related phenomena have also been investigated (e.g., friction during plowing [2], penetration [14], and withdrawing [15]). Through these studies, our understanding of granular friction has been developed. However, these researches have not analyzed the combination of translational and rotational friction.

In addition, some researchers examined frictional drag force exerting on an intruder in a granular bed [16–19]. These researches clarified the friction (drag force) of translational and rolling motion. However, they focused on the drag force within a bulk granular bed. Thus, the details of drag force exerting on an object (sphere) rolling on a granular free surface have not been revealed by these studies.

Some experiments rolling a sphere on a granular surface have been carried out. For example, the dynamics of a sphere rolling down on an inclined rough surface on which grains were glued has been examined [20–22]. Measurement of the friction coefficient has also been performed for the sphere rolling down on a free granular surface. According to Ref. [23], the friction coefficient characterizing energy dissipation is mainly dependent on the sphere's density and almost independent of the motion velocity. This research revealed that the energy dissipation is mainly caused by the sinking of the sphere object. However, a quantitative evaluation of energy dissipation due to the sinking and slipping during the motion has not been carried out. When a basketball or a medicine ball rolls on the granular surface, the friction coefficient characterizing the rolling resistance was estimated by experiments and numerical simulations [24]. However, this
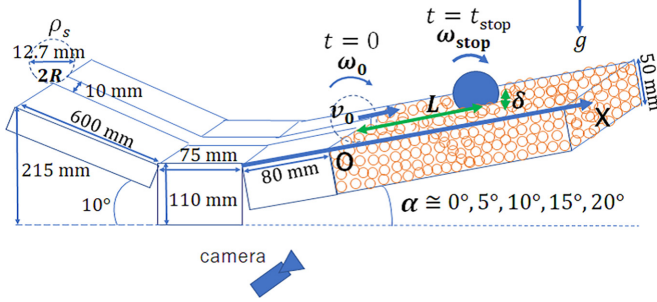
FIG. 1. Experimental setup. By rolling down the slope of the rail made of aluminium, the sphere obtains initial translational velocity v_0 and angular velocity ω_0 when it enters the granular slope at $X = 0$. The sphere rolls up the granular slope from $t = 0$ to $t = t_{\text{stop}}$ (and $X = L$). The X axis is defined along the slope surface. The slope angle is varied from $\alpha \simeq 0°$ to $20°$.

research was conducted under the no-slip situation, so the stuck phenomenon could not be captured. Recently, Texier *et al.* studied the motion of a sphere rolling down on an inclined granular surface [25]. When a sphere was placed on a granular slope, the sphere's behavior depended on the slope angle and density ratio between the sphere and granular matter. They mainly focused on the accelerative motion of the sphere. However, the deceleration of the sphere rolling up a granular slope has not been studied. While the motivation and setup of this study are quite simple, any systematic experiment on the motion of the sphere rolling up a granular slope has not been performed.

Here, we experimentally examine the sphere rolling up a free granular slope to characterize the decelerative motion and to quantify energy dissipation caused by slip motion and groove deformation. To simply discuss energy conservation, rolling-up motion without external driving force is investigated. Although this setup is different from the actual wheel driving situation, the stuck phenomenon, which is characterized by sphere spinning without translational motion, can be mimicked by this simple setup. Using this setup, we characterize the passive (without driving force) stuck motion. We distinguish the friction due to the slipping and shallow sinking (groove formation) of the sphere. And finally, the form to predict rolling-up dynamics is obtained based on energy conservation.

In the next section, the experimental setup, parameters, and other conditions are described. Then, the experimental results (dynamics of the sphere rolling up the slope) are presented in Sec. III and analyzed in Sec. IV. After discussing the physical meaning of the obtained results in Sec. V, the conclusion is provided in Sec. VI.

II. EXPERIMENT

To measure the dynamics of a sphere rolling up a granular slope, we build an experimental apparatus as schematically shown in Fig. 1. A sphere is released at a certain height (160, 180, 200, or 215 mm from the base level) on the rail made of aluminum (rail width: 10 mm). The spheres used in this experiment are made of polyethylene, polyacetal, glass, alumina ceramic, and stainless steel. All these spheres have an

identical radius, $R = 6.35$ mm. Their densities are $\rho_s = 930$, 1400, 2600, 3900, and 7900 kg/m^3, respectively. After rolling down/up the rail, the sphere enters into a glass-beads layer at $X = 0$ at time $t = 0$. The X axis is taken along the surface of the granular layer. The inclination angle α is constant in the region of $X \geqslant -80$ mm. The sphere enters the granular layer with an initial translational velocity $v_0 (= dX/dt$ at $t = 0)$ and initial angular velocity ω_0. Typical diameter of the glass beads used in this experiment is 0.8 mm ($770\,\mu\text{m} - 910\,\mu\text{m}$, AS-One, BZ-08) and the thickness of the granular layer is 50 mm. Granular bulk density in this experiment is estimated as $\rho_g = 1560 \pm 20$ kg/m^3 which corresponds to the packing fraction of $\varphi = 0.64 \pm 0.01$. The inclination angle of the granular slope α is varied as $\alpha \simeq 0°, 5°, 10°, 15°$, and $20°$. By varying α, the effect of gravity on the motion of the sphere changes. The effect of α on translational and rotational slip motions has not been revealed in previous studies. To predict the rolling deceleration under various α conditions, systematic experiments are necessary. Through the systematic experiments conducted in this study, the degree of stuck motion can be characterized.

By varying the releasing position of the sphere, v_0 (and ω_0) can be controlled. Experimental runs with identical conditions are repeated five times to check the reproducibility. Before each experimental run, the granular layer is completely refreshed to ensure the homogeneously flat initial condition. In specific, we remove all glass beads from the box after each experimental run and pour them again. Then, the flat surface is maintained. The mass of glass beads in the box is 1.68 ± 0.02 kg, resulting in $\varphi = 0.64 \pm 0.01$. The dynamics of the sphere's motion during the rolling-up process was captured by a high-speed camera (Omron Sentech, STC-MBS163U3V) with 200 fps and 0.21 mm/pixel resolution (image size: 1080×1440 pixels). From the acquired images, we measure the instantaneous position and rolling posture of the sphere, the maximum travel distance L, and penetration depth δ.

III. RESULTS

Figure 2 shows the images of the sphere rolling up a granular slope (actual movies can be found in the Supplemental Material [26]). By detecting the center of the moving sphere, kinematic data (instantaneous centroid position of the sphere) can be measured. The precise value of the slope angle α is also measured by the sphere's motion. Specifically, α is measured by the slope of the fitting line of positions of the sphere's motion (in the range of $X < 0$). The maximum travel distance L is defined as the distance between $X = 0$ and the position at which the sphere's translational velocity becomes zero. The penetration depth δ is defined by the vertical sinking distance at the final state. We also measure the dynamics of the rolling motion of the sphere. The half of the sphere is colored as shown in Fig. 3. The rolling posture θ ($\theta = 0$ at $t = 0$) of the colored hemisphere is measured with a resolution of 0.017 rad. This measurement resolution is smaller than other error factors. By simply differentiate $\theta(t)$ data, we measure the angular velocity $\omega = d\theta/dt$.

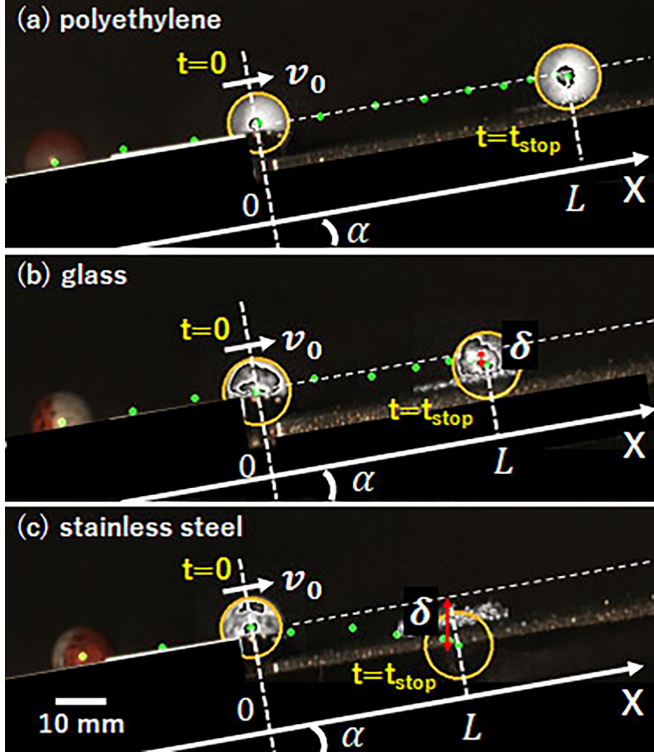When the stainless steel sphere enters the granular layer, it shows significant penetration. The resultant prominent

FIG. 4. The relation between penetration depth δ and inclination angle α. Error bars indicate the standard deviation of various initial velocity cases and five times repeated experimental runs. One can confirm that δ does not show clear dependence on α. The v_0 dependence is also limited in the range of error bars. The penetration depth mainly depends on the density ratio ρ_s/ρ_g.

FIG. 2. The acquired images of the sphere's motions. (a) Polyethylene sphere case: $\alpha = 10.0°$, $v_0 = 0.52$ m/s, $L = 6.0$ cm, and $\delta = 1.01$ mm. (b) Glass sphere case: $\alpha = 9.72°$, $v_0 = 0.43$ m/s, $L = 4.6$ cm, and $\delta = 3.68$ mm. (c) Stainless steel sphere case: $\alpha = 9.60°$, $v_0 = 0.53$ m/s, $L = 4.0$ cm, and $\delta = 11.7$ mm. Yellow circles indicate the circular components identified by the image analysis at $t = 0$ and $t = t_{stop}$. The green dots indicate the centroid position of the sphere motion every 25 ms.

splashing prevents us from the precise identification of the sphere's position as shown Fig. 2(c). Therefore, we cannot analyze the time-resolved dynamics for the stainless steel sphere. In the dynamic analysis, we use the data except for the stainless steel sphere.

A. Penetration depth

First, we characterize the penetration depth of the sphere. By the image analysis of the sphere's motion, final penetration depth δ can be extracted even for the stainless steel sphere
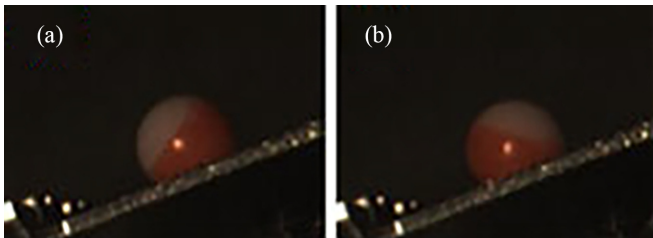

FIG. 3. The snapshot images of polyethylene sphere rolling up a slope of $\alpha \simeq 20°$. The hemispherical part of the sphere is colored in red to measure the rolling posture. The temporal difference between panels (a) and (b) is 5 ms.
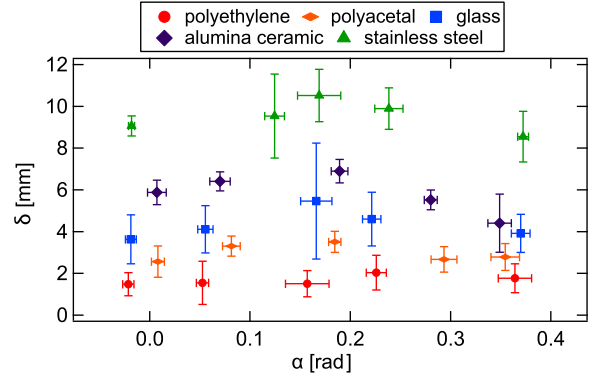
case (as long as the sphere can be detected in the image). The measured δ values for various spheres are plotted in Fig. 4. As seen in Fig. 4, δ value is almost independent of α (and v_0) at least in the range of our experimental conditions. The variation of δ seems to originate from the density difference. Actually, density-dependent penetration depth of a sphere into a granular layer has been investigated in previous works [25,27]. In these studies, the penetration depth of a sphere into a horizontal or inclined granular surface with zero impact velocity was systematically measured. They experimentally found that δ was scaled by the density ratio between sphere and granular layer, ρ_s/ρ_g. Specifically, they proposed a scaling relation,

$$\frac{\delta}{R} = C_\rho \left(\frac{\rho_s}{\rho_g}\right)^{3/4}, \tag{1}$$

where C_ρ is a dimensionless constant. The value of C_ρ was estimated as 0.51 for the penetration into a horizontal granular surface [27] while $C_\rho = 0.61$ was obtained when the sphere was rolling down the granular slope [25]. To check the applicability of this scaling [Eq. (1)] to the case of sphere rolling up a granular slope, the relation between δ/R and ρ_s/ρ_g obtained in this study is plotted in Fig. 5. As expected, the data obtained in this experiment follows the scaling of Eq. (1) with $C_\rho = 0.46$. The data agrees well with the scaling relation. Therefore, we consider that the vertical penetration depth is independent of the surface inclination angle α and the motion in X direction. Although this δ behavior is natural, how this δ scaling affects the entire rolling-up motion is not a trivial problem. Thus, we carefully analyze translational and rotational motions as well.

B. Translational motion

Next, we analyze the translational motion of the sphere rolling up a granular slope. In Fig. 6, the instantaneous position in X direction, $X(t)$, for (a) polyethylene sphere and (b) glass sphere are displayed. Note that $X(t)$ of the stainless steel spheres cannot be measured in many cases due
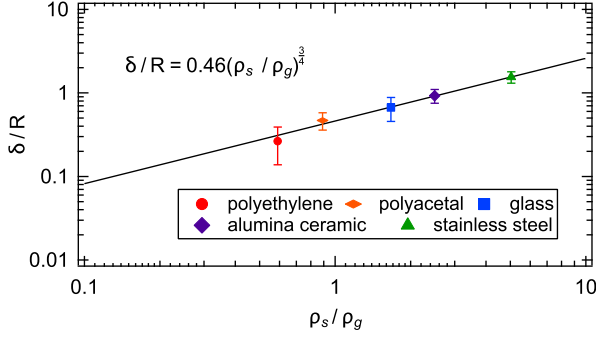
FIG. 5. The double logarithm plot of δ/R vs ρ_s/ρ_g. The solid line indicates the scaling relation [Eq. (1)] with $C_\rho = 0.46$. The value of C_ρ is computed by the least-square fitting. Error bars indicate the standard deviation of all the same ρ_s/ρ_g data (with various v_0 and α cases).

to the deep penetration. Therefore, we analyze the data of polyethylene, polyacetal, glass, and alumina ceramic spheres in the following analysis. And, the data of polyethylene and glass are mainly plotted as representative examples. Although the data of polyacetal and alumina ceramic spheres are not shown in Fig. 6, they also show the similar tendency. As clearly seen in Figs. 6(a) and 6(b), $X(t)$ seems to approach the asymptotic value (maximum travel distance) L. Obviously, L is a decreasing function of inclination angle α.

To characterize the deceleration dynamics, instantaneous velocity $v_X(t)$ is computed by differentiating $X(t)$ data. Typical examples of the $v_X(t)$ data are shown in Figs. 7(a) and 7(b). As observed in Figs. 7(a) and 7(b), constant deceleration can be confirmed both in polyethylene sphere and glass sphere. From the least-square fitting of these data to the linear function, we estimate the average acceleration a_X. The linear trend in $v_X(t)$ behavior can be observed also in all other experimental data. Therefore, we simply assume a_X is constant during the rolling-up process. Actually, more or less similar constant-acceleration behavior was confirmed also in the rolling down experiment [25]. As far as the penetration depth is shallow, the constant acceleration/deceleration seems to be a reasonable approximation to analyze the sphere's motion on the granular slope. However, physical understanding of the constant a_X has not been provided so far and the origin of this constant a_X is still unknown. Although the microscopic (grain-scale) origin of the constant a_X cannot be easily answered, it can be phenomenologically understood on a macroscopic scale. The constant a_X implies that the force exerting on the sphere is constant. To consider the specific energy balance that determines the constant a_X value, we discuss on friction in Sec. IV.

C. Rolling motion

Finally, we analyze the rolling motion. In Figs. 6(c) and 6(d), instantaneous rolling posture $\theta(t)$ is displayed. Here, the posture $\theta(t)$ indicates the inclination of boundary (shown in Fig. 3) driven by rotation in clockwise direction. To characterize the deceleration dynamics of rotation, instantaneous $\omega(t)$ is computed by differentiating $\theta(t)$ data. Typical examples of $\omega(t)$ are shown in Figs. 7(c) and 7(d). From the least-square

fitting of these data to the linear function (from $t = 0$ to t_{stop}), we estimate the average angular acceleration $\dot{\omega}$, where t_{stop} is time at which $v_X = 0$. Similar to the translational motion, constant $\dot{\omega}$ tendency can be confirmed in all experimental data.

By careful inspection of the measured rolling-up movies, we realize that the translational and rolling motions do not halt simultaneously (see the movies in the Supplemental Material [26]). This behavior can be clearly confirmed also in Figs. 7(c) and 7(d). In some cases, rolling motion lasts longer than translational motion. We define this behavior as a stuck phenomenon. Indeed, $\omega_{stop} = \omega(t_{stop})$ is not zero in Fig. 7(d). To clearly show this trend, ω_{stop}/ω_0 is measured and plotted in Fig. 8. One can confirm that ω_{stop}/ω_0 shows an increasing trend with α. We consider ω_{stop}/ω_0 is an indicator characterizing the degree of stuck phenomenon.

According to Ref. [28], when light cylinders rolled on a flat granular bed, the cylinders tended to roll backwards before they completely stopped. In general, translational and rolling motions on granular surfaces do not halt simultaneously. In this experiment, we also observe a time lag between translational and rotational cessations. Both the positive and negative ω_{stop}/ω_0 can be confirmed. The former indicates stuck phenomenon and the latter corresponds to the rolling back motion. To understand these peculiar behaviors, energy dissipation due to friction is considered in the next section.

IV. ANALYSIS

To quantitatively characterize the observed behaviors, we consider two types of energy dissipation models: (i) energy dissipation by granular deformation during translational motion and (ii) energy dissipation due to the slipping friction during rolling motion.

A. Energy dissipation due to deformation of the granular layer

To evaluate energy dissipation due to granular deformation by translational motion of the sphere, energy balance should be considered. Here, we consider a simple energy conservation law between two states: $X = 0$ and L. The energy conservation can be written as

$$\tfrac{1}{2}Mv_0^2 = Mg(L\sin\alpha - \delta) + F_d L, \qquad (2)$$

where the first term of the right-hand side represents the potential energy. To balance the energy budget, the general dissipative term is introduced in the second term of the right-hand side. For the energy dissipation, we simply assume a constant dissipative force F_d. Moreover, F_d can be expressed by the form

$$F_d = \mu_d Mg\cos\alpha, \qquad (3)$$

with an effective friction coefficient μ_d. For the sake of simplicity, we assume μ_d is constant in this study. Note that this μ_d includes the energy dissipation effects such as deformation of the granular surface.
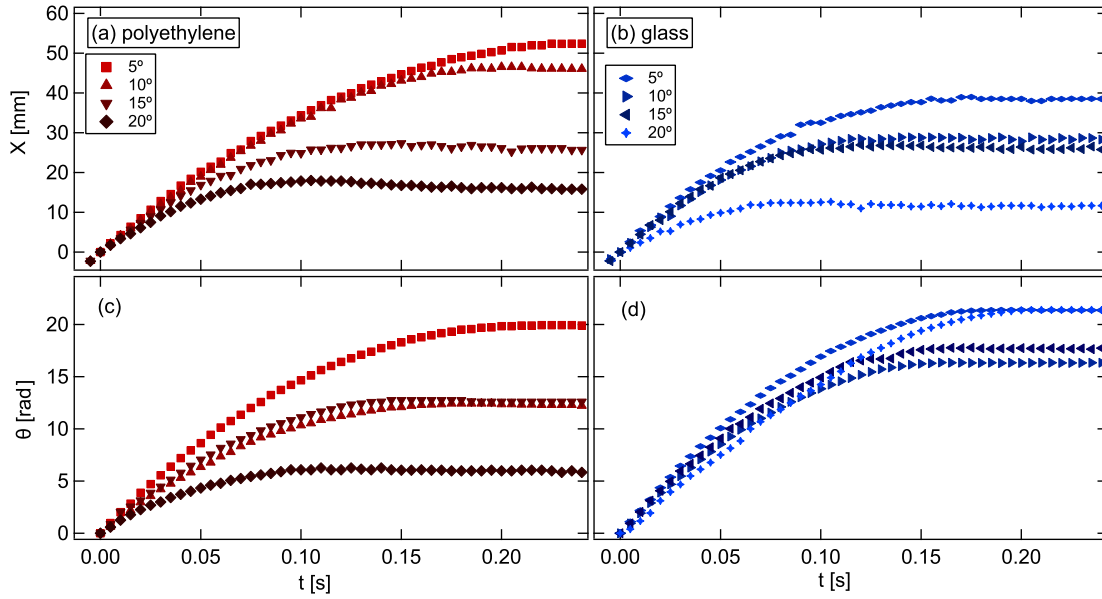
FIG. 6. [(a), (b)] The translational X position and [(c), (d)] the rotational posture θ of the sphere rolling up granular slopes are shown as functions of time. Panels (a) and (c) correspond to polyethylene sphere data and panels (b) and (d) correspond to glass sphere data. The initial velocity for all data shown in this plot is $v_0 \simeq 0.45$ m/s.

From Eqs. (2) and (3), a simple form to estimate the maximum travel distance L can be obtained as

$$L = \frac{v_0^2 + 2g\delta}{2g(\sin\alpha + \mu_d\cos\alpha)}. \qquad (4)$$

Figure 9 shows the experimental result of the relation between L and v_0^2 for polyethylene and glass spheres at $\alpha \simeq 5°$ and $10°$. As can be seen, data are consistent with Eq. (4). Solid lines in Fig. 9 indicate the fitting to Eq. (4). In the fitting, Eq. (1) is substituted into Eq. (4). Then, the intercept of the fitting line is fixed [$(v_0^2, L) = (-2g\delta, 0)$]. The linear relation between L and v_0^2 supports that the sole fitting parameter in this energy conservation equation, μ_d, can be regarded as a constant that is independent of v_0 (and ω_0). This linear trend is confirmed also in all other experimental results. From the fitting of all $L(v_0^2)$ data (with various α and ρ_s cases), we compute μ_d values. The obtained relation between μ_d and α is shown in Fig. 10(a). μ_d is an almost constant value on α.
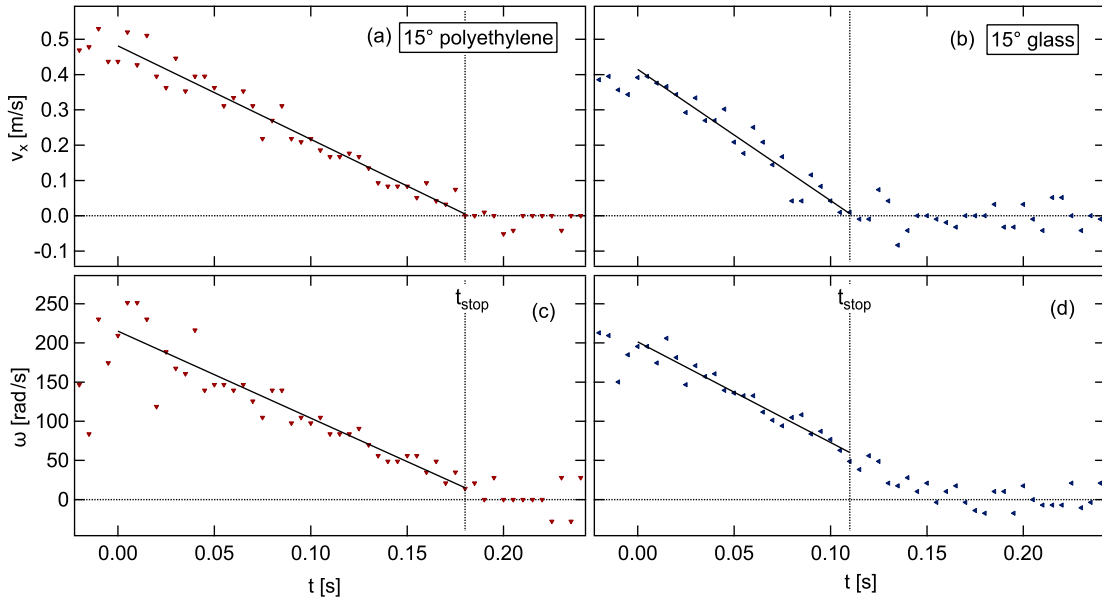

FIG. 7. [(a), (b)] The translational velocity v_X as a function of time t at $\alpha \simeq 15°$ [(a) polyethylene sphere and (b) glass sphere]. By the least-square fitting to the linear deceleration [from $t = 0$ to the stopping time t_{stop} at which $v_X(t_{stop}) = 0$], almost constant deceleration a_X can be obtained. [(c), (d)] The angular velocity $\omega(t)$ as a function of time t at $\alpha \simeq 15°$ [(c) polyethylene sphere and (d) glass sphere]. By the least-square fitting to the linear deceleration (from $t = 0$ to the stopping time t_{stop}), almost constant deceleration $\dot{\omega}$ can be obtained.
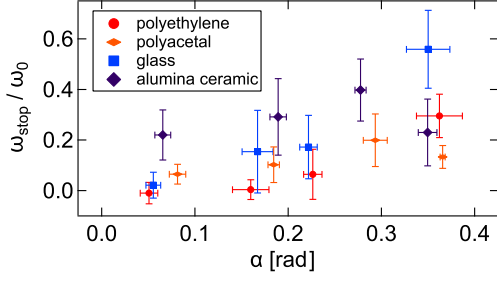
FIG. 8. Measured $\omega_{\text{stop}}/\omega_0$ is plotted as a function of slope angle α. Error bars indicate the standard deviation of the data with various v_0 cases. $\omega_{\text{stop}}/\omega_0 < 0$ means the sphere's rotation originating from the backward translational motion after rotational cessation.

B. Energy dissipation due to the rolling motion

To evaluate dissipation by slipping, a simple rotational equation of motion is considered,

$$I\dot{\omega} = -R\mu_{\text{s}}Mg\cos\alpha, \qquad (5)$$

where $I = (2/5)MR^2$ is the moment of inertia of the homogeneous sphere of mass M and radius R, and μ_{s} is the slipping friction coefficient. Namely, we assume that the deceleration of the rolling motion can be modeled by the simple slipping torque characterized by the constant friction coefficient μ_{s}. Then, the value of μ_{s} can be computed by Eq. (5) and measured $\dot{\omega}$ (other parameters are known). The obtained relation between μ_{s} and α is shown in Fig. 10(b) and the relation between μ_{s} and ρ_s/ρ_g is shown in the inset of Fig. 10(b). It seems that μ_{s} is independent of α and ρ_s/ρ_g. From the obtained data, typical value of μ_{s} is computed as $\mu_{\text{s}} = 0.26 \pm 0.04$.

V. DISCUSSION

In Fig. 10(a), we can confirm μ_{d} is an increasing function of ρ_s/ρ_g. This tendency is similar to the relation between δ/R and ρ_s/ρ_g shown in Fig. 5. As a result, we find a proportional relation,

$$\mu_{\text{d}} = C_{\text{d}}\frac{\delta}{R}, \qquad (6)$$

where $C_{\text{d}} = 0.49$ is a fitting parameter (Fig. 11). Since δ/R is scaled by $(\rho_s/\rho_g)^{3/4}$ [Eq. (1)], this relation is equivalent to $\mu_{\text{d}} \sim (\rho_s/\rho_g)^{3/4}$ shown in the inset of Fig. 11. In general, drag force can be proportional to the contacting or cross-sectional area of the moving object. For example, Pacheco-Vázquez and Ruiz-Suárez revealed the linear relation between the drag force of an intruder into a granular medium and a cross-sectional area [16]. In this regard, Eq. (6) probably means the dissipative granular drag force is proportional to the contact area ($\sim \delta R$) in the current experimental setup. In the translational motion, grains of contacting cross-sectional region have to be removed. Therefore, we consider $\mu_{\text{d}} \propto \delta$. ($R$ is constant in this study.) However, μ_{s} is independent of δ, and the actual slipping surface could be independent of δ. To further discuss the issue, precise measurements of the contacting area and deformed groove are necessary.

When the sphere's density is very large, deep penetration will be observed and the precise measurement of the sphere's

motion becomes quite difficult. In such a situation, even the qualitative behavior might show intrinsically different tendency. In this sense, the frictional characterization discussed so far can be applicable only to the shallow penetration case.

Furthermore, the measured friction coefficients cannot be directly compared with the bulk friction coefficients (as material properties) that are based on the Amontons-Coulomb law (e.g., Ref. [29]). Of course, we consider that the granular friction defined and measured in this study must be different from such conventional ones although all the friction coefficients can be regarded as certain constants under the current experimental conditions. Much more systematic comparison should be performed in the future study.

In addition, there are some restrictions in the current experiment. For example, we do not vary the surface frictional property of the sphere. The experiment with rough-(frictional)-surface spheres is an interesting future problem. Variations of surface property could affect the value of μ_{d} and μ_{s}. Besides, since the sphere is accelerated by rolling over the rail, v_0 and ω_0 are not independent in this experiment. To fully characterize the general stuck phenomena, experiments with independently controlled v_0 and ω_0 should be performed. The shape parameter is also a possible key parameter. Espinosa *et al.* revealed that an imperfect body induces nontrivial motion [30]. The actual surface of the vehicles wheel is not perfectly smooth unlike our research. This point is also a crucial future issue.

Extension of this type of research to the case of the externally driven object (like vehicle wheeling case) would also be important for the practical application to the terramechanics issues. Terramechanics model mainly considers steady motion (without deceleration) although the stuck frequently occurres in actual driving scenes. Therefore, we believe our experimental findings based on changing $v(t)$, $\omega(t)$ are crucial.

Finally, we briefly discuss the application of the current result to the prevention of stuck phenomena related to friction. Since the current experimental system is not driven by torque and normal loading, it is difficult to directly apply our findings to actual stuck problem in vehicle driving. However, according to Fig. 8, the degree of slipping rotation after the translational cessation increases as the α increases. This means that the risk of stuck occurrence (without any driving accelerator) increases when the sphere tries to roll up the steeper slope. To reduce the degree of stuck, α should be small. In this study, the degree of stuck motion for the passively rolling sphere is quantitatively measured for the first time.

Besides, by using the empirical law, $\mu_{\text{d}} = 0.49(\delta/R)$, we can predict sphere motion at any time. In specific, we can predict the maximum travel distance L by using Eqs. (1) and (4) in arbitrary initial conditions. As discussed so far, the sphere is rolling up with a constant deceleration a_X, until $t = t_{\text{stop}}$, satisfying $v(t) = v_0 - \frac{v_0^2}{2L}t$. Regarding the rotational motion, $\omega(t)$ can be computed by Eq. (5) with $\mu_{\text{s}}(\simeq 0.26 \pm 0.04)$. Then, the sphere's motion both in translational and rotational directions can be completely computed. That is, in this study, we find some useful relations for the sphere's motion on a granular slope by obtaining parameters μ_{d} and μ_{s}.
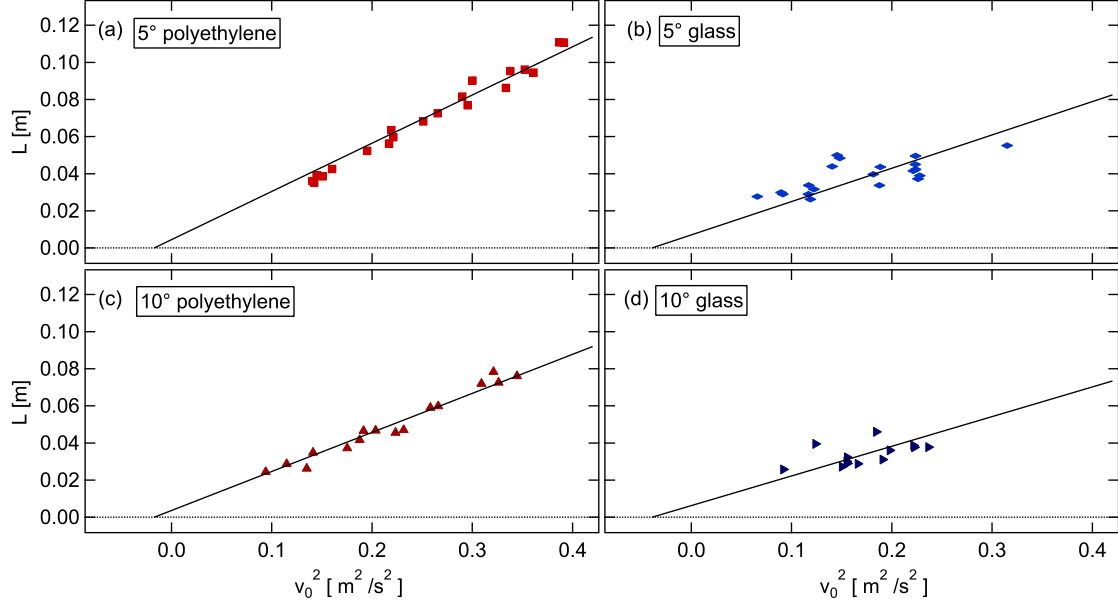
FIG. 9. The relations between L and v_0^2 are plotted. The solid lines denote the fitting through the fixed point $(v_0^2, L) = (-2g\delta, 0)$. The value of δ is computed based on Eq. (1). The positive L value at $v_0 = 0$ comes from the effect of inclination and the definition. (a) 5° polyethylene sphere, (b) 5° glass sphere, (c) 10° polyethylene sphere, and (d) 10° glass sphere. From the gradient of the fitting line, μ_d can be estimated using Eq. (4).

VI. CONCLUSION

This study reveals the dynamics of a sphere rolling up a granular slope. By systematically varying the initial velocity v_0 (and initial angular velocity ω_0), angle of slope α, and density ratio between the sphere and granular layer ρ_s/ρ_g, the sphere's motion was measured and analyzed. First, the penetration depth of the sphere during the rolling-up process was measured and scaled as $\delta/R = C_\rho (\rho_s/\rho_g)^{3/4}$. This scaling is consistent with previous studies of the sphere penetration into a granular layer. Next, translational and rotational
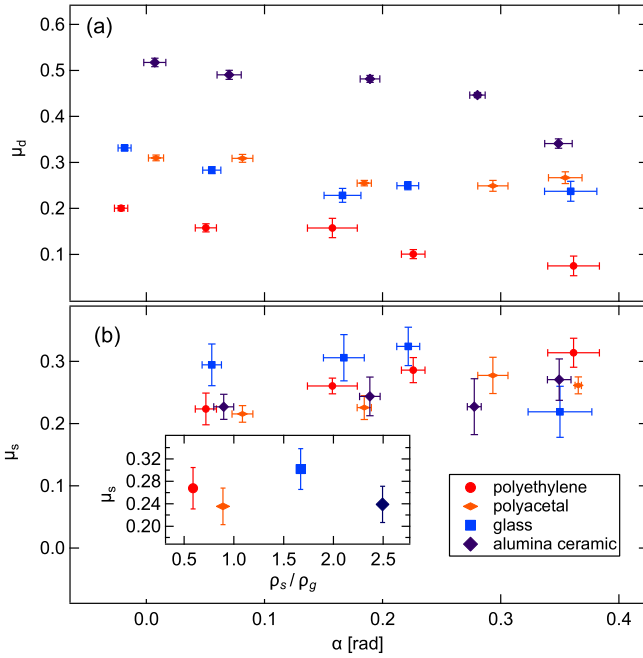

FIG. 10. (a) Friction coefficient characterizing translational energy dissipation μ_d and (b) friction coefficient due to the slipping μ_s are plotted vs α. Error bars indicate the standard deviation of the data with various v_0 cases and repeated experiments. In the inset of panel (b), μ_s are plotted vs ρ_s/ρ_g. Error bars indicate the standard deviation of the all the same ρ_s/ρ_g data (with various v_0 and α cases).
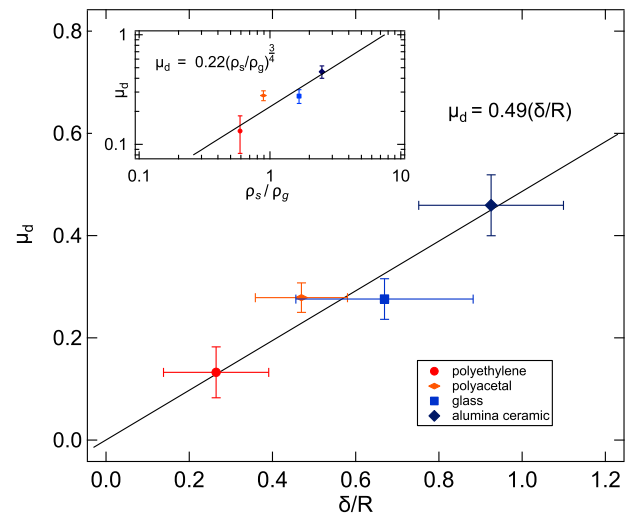
FIG. 11. The relation between μ_d and δ/R is plotted. By the least-square fitting, the proportional relation between μ_d and δ/R is obtained. Error bars indicate the standard deviation of all the same ρ_s/ρ_g data (with various v_0 and α cases). In the inset, the double logarithm plot of μ_d vs ρ_s/ρ_g is shown. The solid line indicates scaling relation.

motions of the rolling-up sphere are measured and characterized as constant deceleration dynamics. Then, we reveal that ω_{stop} increases with α. To characterize the sphere's motion, we consider two kinds of friction coefficients, μ_{d} and μ_{s}. The former and latter represent friction due to the deformation of granular layer and slipping friction, respectively. We obtain the relation, $\mu_{\text{d}} = 0.49(\delta/R)$, meaning the contact area between the sphere and granular layer is a key factor of translational energy dissipation. The μ_{s} is almost independent of α and ρ_s/ρ_g, showing a constant value $\mu_{\text{s}} \simeq 0.26 \pm 0.04$. From the system parameters, ρ_s/ρ_g, R and α, we can estimate δ and μ_{d}. Then, by considering constant μ_{s} and initial conditions v_0

(ω_0), we can completely predict the sphere's rolling-up motion. Since the range of ρ_s/ρ_g variation is limited in this study, more systematic experiments with wider parameter ranges are crucial future problem.

[1] H. Katsuragi, *Physics of Soft Impact and Cratering* (Springer, Berlin, 2016).

[2] N. Gravish, P. B. Umbanhowar, and D. I. Goldman, Phys. Rev. Lett. **105**, 128301 (2010).

[3] G.-G. Jorge and J. C. Ruiz-Suárez, Eur. Phys. J. E **40**, 45 (2017).

[4] K. Sanderson, Nature (London) **463**, 600 (2010).

[5] M. Sutoh, R. Yajima, K. Nagatani, and K. Yoshida, *Proc. IEEE/SICE Int. Symp. on System Integration* (IEEE, Piscataway, NJ, 2011), pp. 884–889.

[6] M. Sutoh, K. Nagaoka, K. Nagatani, and K. Yoshida, *Proc. IEEE Int. Conf. on Robotics and Automation* (IEEE, Piscataway, NJ, 2012), pp. 3419–3424.

[7] A. Fertin and J. Casas, J. Exp. Biol. **209**, 3510 (2006).

[8] J. Crassous, A. Humeau, S. Boury, and J. Casas, Phys. Rev. Lett. **119**, 058003 (2017).

[9] P. Senthil Kumar, U. Sruthi, N. Krishna, K. J. P. Lakshmi, R. Menon, Amitabh, B. Gopala Krishna, D. A. Kring, J. W. Head, J. N. Goswami *et al.*, J. Geophys. Res. Planets **121**, 147 (2016).

[10] A. Ikeda, H. Kumagai, and T. Morota, J. Geophys. Res. Planets **127**, e2021JE007176 (2022).

[11] O. Pouliquen, C. Cassar, P. Jop, Y. Forterre, and M. Nicolas, J. Stat. Mech. (2006) P07020.

[12] F. da Cruz, S. Emam, M. Prochnow, J.-N. Roux, and F. Chevoir, Phys. Rev. E **72**, 021309 (2005).

[13] O. Kuwano, R. Ando, and T. Hatano, Geophys. Res. Lett. **40**, 1295 (2013).

[14] M. Schröter, S. Nägle, C. Radin, and H. L. Swinney, Europhys. Lett. **78**, 44004 (2007).

[15] T. Furuta, S. Kumar, K. A. Reddy, H. Niiya, and H. Katsuragi, New J. Phys. **21**, 023001 (2019).

[16] F. Pacheco-Vázquez and J. C. Ruiz-Suárez, Phys. Rev. E **80**, 060301(R) (2009).

[17] T. A. Brzinski III and D. J. Durian, Soft Matter **6**, 3038 (2010).

[18] V. L. Díaz-Melián, A. Serrano-Muñoz, M. Espinosa, L. Alonso-Llanes, G. Viera-López, and E. Altshuler, Phys. Rev. Lett. **125**, 078002 (2020).

[19] S. Agarwal, D. I. Goldman, and K. Kamrin, Proc. Natl. Acad. Sci. USA **120**, e2214017120 (2023).

[20] M. A. Aguirre, I. Ippolito, A. Calvo, C. Henrique, and D. Bideau, Powder Technol. **92**, 75 (1997).

[21] C. Henrique, M. A. Aguirre, A. Calvo, I. Ippolito, S. Dippel, G. G. Batrouni, and D. Bideau, Phys. Rev. E **57**, 4743 (1998).

[22] G. L. Vasconcelos and J. J. P. Veerman, Phys. Rev. E **59**, 5641 (1999).

[23] F. V. De Blasio and M.-B. Saeter, Phys. Rev. E **79**, 022301 (2009).

[24] S. V. Wal, S. Tardivel, P. Sánchez, D. Djafari-Rouhani, and D. Scheeres, Granular Matter **19**, 17 (2017).

[25] B. D. Texier, A. Ibarra, F. Vivanco, J. Bico, and F. Melo, Europhys. Lett. **123**, 54005 (2018).

[26] See Supplemental Material at http://link.aps.org/supplemental/10.1103/PhysRevE.109.014903 for videos of rolling spheres on a granular slopes.

[27] J. S. Uehara, M. A. Ambroso, R. P. Ojha, and D. J. Durian, Phys. Rev. Lett. **90**, 194301 (2003).

[28] K. J. Burns, N. J. Balmforth, and I. J. Hewitt, Proc. R. Soc. A **473**, 20170375 (2017).

[29] H. Kawamura, T. Hatano, N. Kato, S. Biswas, and B. K. Chakrabarti, Rev. Mod. Phys. **84**, 839 (2012).

[30] M. Espinosa, L. Martínez-Ortíz, L. Alonso-Llanes, L. A. R. de Torner, O. Chávez-Linares, and E. Altshuler, Sci. Adv. **9**, eadf6243 (2023).